Environmental Pollution 335 (2023) 122282

Contents lists available at ScienceDirect

Environmental Pollution

journal homepage: www.elsevier.com/locate/envpol

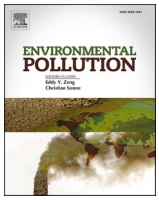

Small polystyrene microplastics interfere with the breakdown of milk proteins during static *in vitro* simulated human gastric digestion☆

Maria Krishna de Guzman [a,b], Dragana Stanic-Vucinic [c], Nikola Gligorijevic [d], Lukas Wimmer [e], Manvel Gasparyan [f,g], Tamara Lujic [c], Tamara Vasovic [c], Lea Ann Dailey [e], Sam Van Haute [a,b], Tanja Cirkovic Velickovic [a,b,c,h,*]

[a] Department of Food Technology, Safety, and Health, Faculty of Bioscience Engineering, Ghent University, Ghent, Belgium
[b] Center for Food Chemistry and Technology, Ghent University Global Campus, Incheon, Republic of Korea
[c] Center of Excellence for Molecular Food Sciences, Department of Biochemistry, University of Belgrade – Faculty of Chemistry, Belgrade, Serbia
[d] Department of Chemistry, University of Belgrade – Institute of Chemistry, Technology and Metallurgy, National Institute of Republic of Serbia, Belgrade, Serbia
[e] Department of Pharmaceutical Sciences, University of Vienna, Vienna, Austria
[f] Center for Biosystems and Biotech Data Science, Ghent University Global Campus, Republic of Korea
[g] School of Environmental Engineering, University of Seoul, Seoul, Republic of Korea
[h] Serbian Academy of Sciences and Arts, Belgrade, Serbia

ARTICLE INFO

Keywords:
Microplastics
Polystyrene
Pepsin
Enzyme activity
Simulated gastric digestion
Cow's milk

ABSTRACT

Human ingestion of microplastics (MPs) is common and inevitable due to the widespread contamination of food items, but implications on the gastric digestion of food proteins are still unknown. In this study, the interactions between pepsin and polystyrene (PS) MPs were evaluated by investigating enzyme activity and conformation in a simulated human gastric environment in the presence or absence of PS MPs. The impact on food digestion was also assessed by monitoring the kinetics of protein hydrolysis through static *in vitro* gastric digestion of cow's milk contaminated with PS. The binding of pepsin to PS showed that the surface chemistry of MPs dictates binding affinity. The key contributor to pepsin adsorption seems to be π−π interactions between the aromatic residues and the PS phenyl rings. During quick exposure (10 min) of pepsin to increasing concentrations (222, 2219, 22188 particles/mL) of 10 μm PS (PS10) and 100 μm PS (PS100), total enzymatic activities were not affected remarkably. However, upon prolonged exposure at 1 and 2 h, preferential binding of pepsin to the small, low zeta-potential PS caused structural changes in the protein which led to a significant reduction of its activity. Digestion of cow's milk mixed with PS10 resulted in transient accumulation of larger peptides (10–35 kDa) and reduced bioavailability of short peptides (2–9 kDa) in the gastric phase. This, however, was only observed at extremely high PS10 concentration (0.3 mg/mL or 5.46E+05 particles/mL). The digestion of milk peptides, bound preferentially over pepsin within the hard corona on the PS10 surface, was delayed up to 15 min in comparison to bulk protein digestion. Intact caseins, otherwise rapidly digested, remained bound to PS10 in the hard corona for up to 15 min. This work presents valuable insights regarding the interaction of MPs, food proteins, and pepsin, and their dynamics during gastric digestion.

1. Introduction

The presence of microplastics (MPs) in the environment and their transfer into the food chain and human body has attracted significant attention from the scientific community, government agencies, and the general population. Ingestion or oral exposure is one of the major ways that humans are exposed to microplastics (Galloway, 2015). Hence, research efforts have focused on MP contamination of several food items

Abbreviations: (MPs), Microplastics; (PS), polystyrene; (PS10), 10 μm PS; (PS100), 100 μm PS; (SGF), simulated gastric fluid; (SSF), simulated salivary fluid; (Hb), hemoglobin; (GIT), gastrointestinal tract; (PM), pepsin and milk; (PMPS1), pepsin and milk mixed with 3.9E-03 mg/mL PS10; (PMPS2), pepsin and milk mixed with 0.3 mg/mL PS10.

☆ This paper has been recommended for acceptance by Maria Cristina Fossi.

* Corresponding author.#925 Ghent University Building, Incheon Global Campus, 119-5 Songdomunhwa-ro, Yeonsu-gu, Incheon, 21985, Republic of Korea.
E-mail address: tcirkov@chem.bg.ac.rs (T. Cirkovic Velickovic).

https://doi.org/10.1016/j.envpol.2023.122282
Received 15 May 2023; Received in revised form 12 July 2023; Accepted 27 July 2023
Available online 27 July 2023

and beverages (EFSA, 2016).

Drinking water is the most highly studied beverage, especially bottled water,owing to its high consumption worldwide (Pivokonsky et al., 2018; Zuccarello et al., 2019; Kankanige & Babel, 2020; Tong, Jiang, Hu, & Zhong, 2020; Chanpiwat & Damrongsiri, 2021; Makhdoumi et al., 2021; Zhou et al., 2021). Bottled water was found to have a higher MP content (10.4 particles/L) compared to tap water (5.45 particles/L) due to the migration of debris from the plastic containers and caps (Mason et al., 2018; Pivokonsky et al., 2018; Kankanige & Babel, 2020). However, MP contamination coming from water treatment and packaging processes should not be overlooked since even drinking water packaged in glass bottles has also been reported to contain MPs (Jin et al., 2021). Other commonly consumed beverages such as milk, tea, beer, wine, and soft drinks were also previously reported to be contaminated (Hernandez et al., 2019; Diaz-Basantes et al., 2020; Prata et al., 2020; Shruti et al., 2020). In these products, water is the main ingredient and majority of the MPs most likely came from this source (Shruti et al., 2020).

The highest reported MP contamination in beverages comes from plastic containers in combination with thermal processing, such as heated tea or coffee cups and infant polypropylene (PP) bottles (Li et al., 2020; Schwabl, 2020; Ranjan et al., 2021). Around 25,000 Nile-red tagged MPs per 100 mL water were released from disposable paper cups, and even more MPs were detected from sterilized infant PP bottles and accessories (Li et al., 2020). Recently, a greater focus has also been given to terrestrially grown products, such as fruits and vegetables. In 2020, Conti et al. reported that carrot samples contained the highest number of MPs (<10 μM) compared to lettuce, broccoli, and potatoes, while apples were found to be more contaminated than pears. Fruits (median 223,000 particles/gram) contained more MPs than vegetables (median 97,800 particles/gram) due to the larger size and network of vascularization in fruit trees.

Despite the extensive documentation of food contamination by MPs, there is still limited information regarding their behavior in complex fluid mixtures in the gastrointestinal tract (GIT). MPs come into contact with the GIT the moment contaminated food and beverages enter the mouth. Reports on gut homeostasis, toxicity, cellular uptake, and translocation of MPs are available (Hirt and Body-Malapel, 2020; Dong et al., 2023), but these studies mostly focused on the cellular component while digestive fluids and enzymes necessary to breakdown food are overlooked. To date, only gastric lipid digestion has been examined where lipase activity and lipid digestion were both inhibited by MPs (Tan et al., 2020). Food proteins, however, have not yet been explored. This group of macronutrients is not only an important source of bioactive peptides and essential amino acids, but it can also exhibit adverse effects in humans, particularly in susceptible individuals (food allergies, celiac disease, and food intolerances).

Hence, in this study, we focused on pepsin, the major protease in the stomach (Goodsell et al., 2015), its affinity to and behavior in the presence of 10 μm and 100 μm PS MPs, and the digestion of cow's milk proteins. PS is the most prominent MP in Korean clams (de Guzman et al., 2022) and it is one of the most highly manufactured polymers globally (Erni-Cassola et al., 2019). Cow's milk is an important source of proteins, and also one of the most important sources of food allergens (Gendel and Zhu, 2013). Implications on the specific activity and conformation of pepsin during and after exposure to PS were investigated. Furthermore, consequences of PS on the breakdown of proteins were explored using liquid cow's milk subjected to *in vitro* simulated human oral and gastric digestion (Brodkorb et al., 2019). This study provides first evidence of a possible impairment of protease activity and protein digestion by PS MPs.

2. Materials and methods

2.1. Reagents, materials, and equipment

Pepsin from porcine gastric mucosa (Sigma-aldrich, P7012-5G) was used in all enzymatic experiments. Monodispersed microparticle standards of PS10 (Sigma-Aldrich, 72822-10 ML-F) and PS100 (Sigma-Aldrich, 59336-5 ML-F) were purchased as 2% w/v suspensions of known particle concentrations. Hemoglobin (Hb) (Sigma-Aldrich, H6525-25G) served as a substrate for the enzyme activity assay, while 5% w/v trichloroacetic acid (TCA, Sigma-Aldrich, T6399-5G) was used to stop the reaction. Ultrafree® MC-HV centrifugal filters, 0.45 μm (UFC30HVNB, Merck Millipore, Cork, Ireland), were used to separate PS beads from the solution. The concentration of pepsin was measured using a Pierce™ BCA protein assay kit (23225, ThermoFisher scientific, Massachusetts, USA).

Absorbance values were recorded using a Jenway 7315 UV–Visible spectrophotometer (Cole-Parmer, Illinois, USA), while Thermo Scientific Nicolet iS5 FTIR with iD7ATR (ThermoFisher Scientific, Massachusetts, USA) was used to collect FTIR spectra. SEM analysis was performed using a FEI/Philips XL30 ESEM (FEI, Oregon, USA). SDS-PAGE and gel imaging were conducted using a Bio-Rad Mini-PROTEAN tetra cell and Bio-Rad ChemiDoc XRS+ with Imagelab™ software (Bio-Rad, California, USA), respectively. Far and near UV CD spectra were recorded on a J-815 CD spectropolarimeter (JASCO, Tokyo, Japan). Intrinsic tryptophan fluorescence was acquired using FluoroMax-4 spectrofluorometer (Horiba Scientific, Kyoto, Japan). Zeta potential measurements were performed using a Malvern Zetasizer Nano ZS (Malvern Panalytical, Worcestershire, UK) with disposable folded capillary cells (DTS1070), while data was analyzed with the Zetasizer Software (VN: January 8, 4906, Malvern Panalytical, Worcestershire, UK).

2.2. Pepsin activity assay

The specific activity of pepsin was determined using a spectrophotometric stop reaction based on Anson and Mirsky (1932) where Hb was used as substrate. One unit of activity corresponds to ΔA_{280} of 0.001 per minute. This experiment was conducted in two formats – (1) quick (10 min) exposure to PS before addition of the Hb substrate, and (2) 1 h (1h) and 2 h (2h) exposure to PS with subsequent removal of the beads before the addition of Hb. In the first format, MPs, enzyme, and substrate were all present in the mixture during the reaction. The second format allows close examination of the interaction between PS and pepsin for a longer period of time (1h and 2h). Enzymatic activity was determined at pH 2 while simulated gastric fluid (pH 3) was based on Infogest 2.0 (composition of SGF is in Table S1 of SI) (Brodkorb et al., 2019).

In the first format, a 40 μL aliquot of PS10 or PS100 (in SGF), with three different particle counts: (1) low- 142 particles, (2) moderate- 1420 particles, and (3) high- 14200 particles, were added to 100 μL of five different pepsin solutions having a concentration between 5 and 25 μg/mL. The low particle count was based on the average daily MP consumption estimated by Cox et al. (2019). After 10 min of incubation at 37 °C (with gentle shaking), 500 μL of 2% w/v Hb, pH 2, was added. At this point, the PS concentrations were: (1) low- 222 particles/mL, (2) moderate- 2219 particles/mL, and (3) high- 22188 particles/mL. The corresponding mass concentrations for PS10 were: (1) low- 0.12 μg/mL, (2) moderate- 1.22 μg/mL, and (3) high- 12.20 μg/mL. For PS100, the mass concentrations were as follows: (1) low- 122.0 μg/mL, (2) moderate- 1219.8 μg/mL, and (3) high- 12198.2 μg/mL. The surface area per unit volume of PS10 was (1) low- 6.97E-04 cm^{-}, (2) moderate- 6.97E-03 cm^{-}, and (3) high- 6.97E-02 cm^{-}, while the following was for PS100: (1) low- 6.97E-02 cm^{-}, (2) moderate- 6.97E-01 cm^{-}, and (3) high- 6.97 cm^{-}. This mixture of pepsin, Hb, PS10/PS100 was allowed to react for 10 min at 37 °C (with gentle shaking). A mixture containing only Hb and pepsin were incubated at the same time to serve as control. To stop the

reaction, 1 mL 5% w/v TCA was added followed by centrifugation at 6000×*g* for 30 min. The PS beads were removed from the supernatant using 0.45 μm filters. The control was filtered in the same way to account for loss of peptides due to binding on the filter. The absorbance of TCA-soluble tyrosine-containing peptides was measured at 280 nm. A blank solution was prepared by first mixing Hb and TCA followed by the addition of pepsin. Final total pepsin activity was calculated by taking the average total activity of the five different pepsin concentrations.

In the second case, 0.3 mL of 0.167 mg/mL pepsin (in SGF) was mixed with 0.2 mL of PS10/PS100 (in SGF) to give a final concentration of 0.1 mg/mL pepsin, and 222 (low PS), 2219 (moderate PS), and 22188 (high PS) particles/mL PS, which is the same concentrations used in the first case after addition of Hb substrate. This gives a pepsin:PS10 mass ratio of 820, 82, and 8.2. In the case of PS100, the pepsin:PS mass ratios were 0.82, 0.082, and 0.0082. After 1h and 2h of pepsin exposure to PS at 37 °C (with gentle shaking), particles were removed using 0.45 μm filters. Corresponding 0h, 1h, and 2h pepsin controls (without PS) were treated in the same way. Pepsin activity was determined by reacting 100 μL of the resulting pepsin solutions to 0.5 mL of Hb for 10 min at 37 °C (with gentle shaking). The reaction was terminated with TCA and absorbance was measured as previously described. There were six different replicates for each level of PS concentration (low, moderate, high) and each level of exposure time (0h, 1h, 2h). The total and specific enzyme activities were determined by taking the average of the six replicates. To calculate the specific activity, the protein content in the filtered solutions, after 1h and 2h exposure to PS, was measured using microBCA protein assay following manufacturer's protocol.

2.3. Circular dichroism and fluorescence spectroscopy

Pepsin was incubated with PS10 and PS100 in SGF for 1h and 2h at a concentration of 685 μg/mL for both pepsin and MPs, resulting in a 1:1 mass ratio. After removing the PS beads, CD spectra were collected using a 0.1 mm path length cell in the far UV region (190–260 nm) and a 10 mm path length cell in the near UV region (260–320 nm) with a scan rate of 50 nm/min and accumulation of three scans. The spectra were corrected by subtracting the buffer spectra, and the ellipticity values were converted into molar ellipticity using the following equation:

$$[\theta] = \frac{\theta \, x \, Mr}{C \, x \, l \, x \, 10}$$

where *[θ]* is molar ellipticity in mdeg x cm^2/dmol, *Mr* is molar weight of pepsin (35000 Da), *C* is concentration of pepsin that remained in solution after incubation with PS, and *l* is path length of cell (0.01 cm for far and 1 cm for near UV CD).

Secondary structure content was calculated by transforming molar ellipticity from far UV CD spectra to molar ellipticity per residue by dividing [θ] values with the number of amino acids in pepsin (326). Obtained data was then analyzed by CONTIN algorithm in CDpro software. SP29 was used as database.

The intrinsic fluorescence spectra of the same pepsin solutions were recorded at room temperature using a quartz cuvette with 1 cm path length at an excitation wavelength of 280 nm and emission range from 290 to 450 nm. The final concentration of pepsin and MPs was 32.5 mg/mL (mass ratio 1:1). Slits were set at 5 nm for both excitation and emission. Obtained emission spectra were corrected by subtraction of spectra obtained from the buffer.

2.4. Static in vitro digestion of milk proteins

Cow's milk (Korean brand Maeil) was subjected to static *in vitro* oral and gastric digestion based on Infogest 2.0 (Brodkorb et al., 2019). Centrifugation was conducted at 4000×*g* for 30 min at 4 °C prior to the experiment to further reduce the fat content of the sample. The final fat content was determined by a gravimetric method (Section S1 of SI) and was estimated to be 0.5g/100 mL. Simulated salivary fluid (SSF) and SGF were also prepared beforehand following Infogest 2.0 protocol. The composition of the simulated fluids is shown in Table S1.

The following sets were prepared to serve as controls: (1) M-milk only, (2) P- pepsin only, and (3) PM-pepsin and milk. For the first experimental set (PMPS1), pepsin and milk were spiked with high (14200 particles) PS10, resulting to a concentration of 3.9E-03 mg/mL PS (7.1E+03 particles/mL) in the final gastric mixture. A total of 8 tubes were prepared for each treatment, each tube corresponding to the following time points of gastric digestion: 5, 10, 15, 20, 30, 60, 90, and 120 min. This was done to monitor the progress of protein breakdown in the sample. During the oral phase, 0.5 mL of milk or DI water was mixed with 0.5 mL of SSF and incubated while mixing for 2 min at 37 °C. Salivary amylase was not added to SSF since the sample did not contain starch. At the end of the oral phase, the pH of the oral bolus was measured and adjusted to 3.0 before proceeding to the gastric phase.

In the gastric phase, the oral bolus was diluted with SGF to reach a final ratio of 1:1 (v/v). Porcine pepsin solution was added at 0.685 mg/mL, which gives an activity of 2000 U/mL in the final mixture. DI water was added instead of pepsin solution in the control set containing milk only. Right after the addition of pepsin, the mixture was incubated for 5, 10, 15, 20, 30, 60, 90, and 120 min with mixing at 37 °C. The pH was adjusted to 7.0–8.0 at the end of the different incubation times to inactivate pepsin. For solutions containing PS, beads were removed using centrifugal filters after pepsin inactivation. Solutions were kept at 4 °C prior to SDS-PAGE or at −20 °C when overnight storage was necessary.

A second experimental set (PMPS2) was prepared in the same way as described above, but the quantity of spiked PS10 was increased from 1.42E+04 (3.9E-03 mg/mL) to 1.09E+06 particles. This gives a final concentration of 0.3 mg/mL PS or 5.46E+05 particles/mL in the final gastric mixture.

After gastric digestion, digesta from all timepoints were analyzed by SDS-PAGE as described in Section S2. The PS beads were also collected, and the protein corona was extracted according to Section S3 and further analyzed by SDS-PAGE.

2.5. Data analysis

Enzyme activities are reported as total activity (Units, U) or specific activity (Units per mg, U/mg). Final activities are expressed as mean ± SEM (standard error of the mean). SPSS statistics 26.0.0.0. was used for statistical analysis. Equality of variance among treatment groups was first tested using Levene's test. Differences between treatments (i.e., size of PS, concentration of PS, and exposure time) were determined by one-way ANOVA when variance was equal, or Brown-Forsythe test when variance was unequal. Tukey HSD was performed right after ANOVA, while Games-Howell test was conducted following Brown-Forsythe test (significance level of $p < 0.05$) when post hoc test was applicable.

3. Results

3.1. Characterization of PS beads

Commercial PS10 and PS100 particles were first characterized by ATR-FTIR, SEM, and zeta potential analysis as described in Section S4 of SI. The polymer identity matches the reference spectrum of low molecular weight polystyrene with a match score of 63.53 for PS10 and 64.64 for PS100 (Fig. 1A). As expected, both sizes of PS were in the form of beads or spheres, and particle surface was smooth and not porous (Fig. 1B and C). Visible residue on the surface of the beads most likely came from the solvent which was dried-off prior to SEM.

The corresponding weights and total surface area of different concentrations of PS10 and PS100 are shown on Table S2 and S3. These values were calculated as described in Section S5 and S6 of SI. The mass of PS100 was always 1000 times higher than PS10 at the same particle

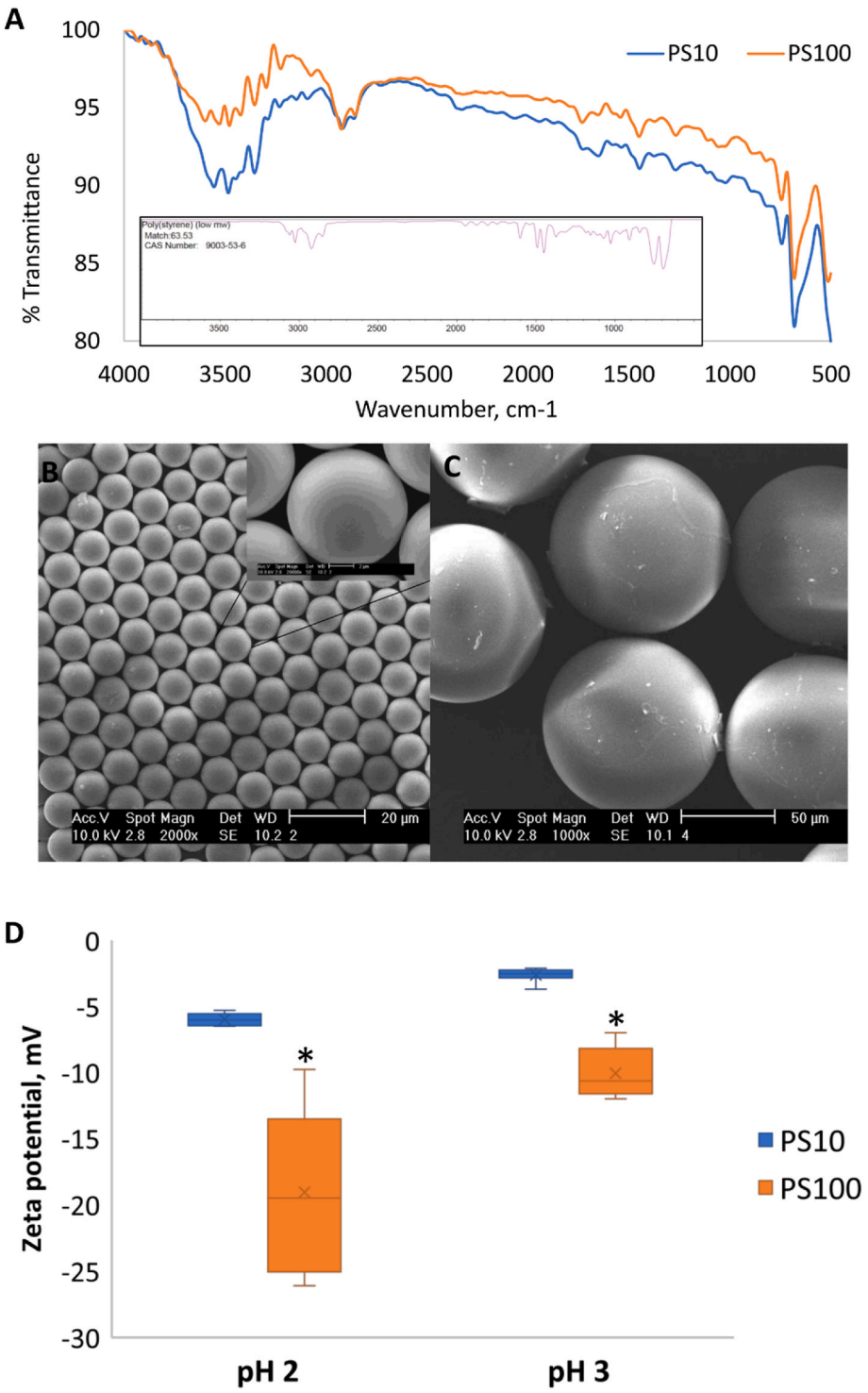

Fig. 1. Characterization of PS beads. (A) FTIR spectra of PS10 and PS100. Inset shows the reference spectrum of low molecular weight PS; SEM images of (B) PS10 and (C) PS100; (D) Zeta potential of PS10 and PS100 at pH 2 (10 mM HCl) and pH 3 (SGF). (*) denotes significant difference at $p < 0.05$.

count due to the larger diameter of PS100. Similarly, the total surface area was always 100 times larger for PS100 compared to PS10. Low PS100 and high PS10 have the same surface area at 4.5E-02 cm^2. Zeta potential analysis revealed a slight negative charge at pH 2 and pH 3 as illustrated in Fig. 1D. PS100 consistently showed a significantly negative ($p < 0.05$) zeta potential compared to PS10 for both pH levels. However, in terms of stability, this difference is negligible since the values are not higher than ±30 mV (Clogston and Patri, 2011).

3.2. Changes in pepsin activity

The pepsin activity was determined using two different approaches. In the first approach, pepsin and PS were shortly incubated (10 min) in SGF, followed by the reaction with Hb substrate for another 10 min. Fig. 2A shows that increasing concentrations of PS10/PS100 did not significantly affect pepsin activity during the 10-min exposure. This suggests that PS size and concentration had no effect on enzyme performance during this short contact period. Furthermore, displacement of

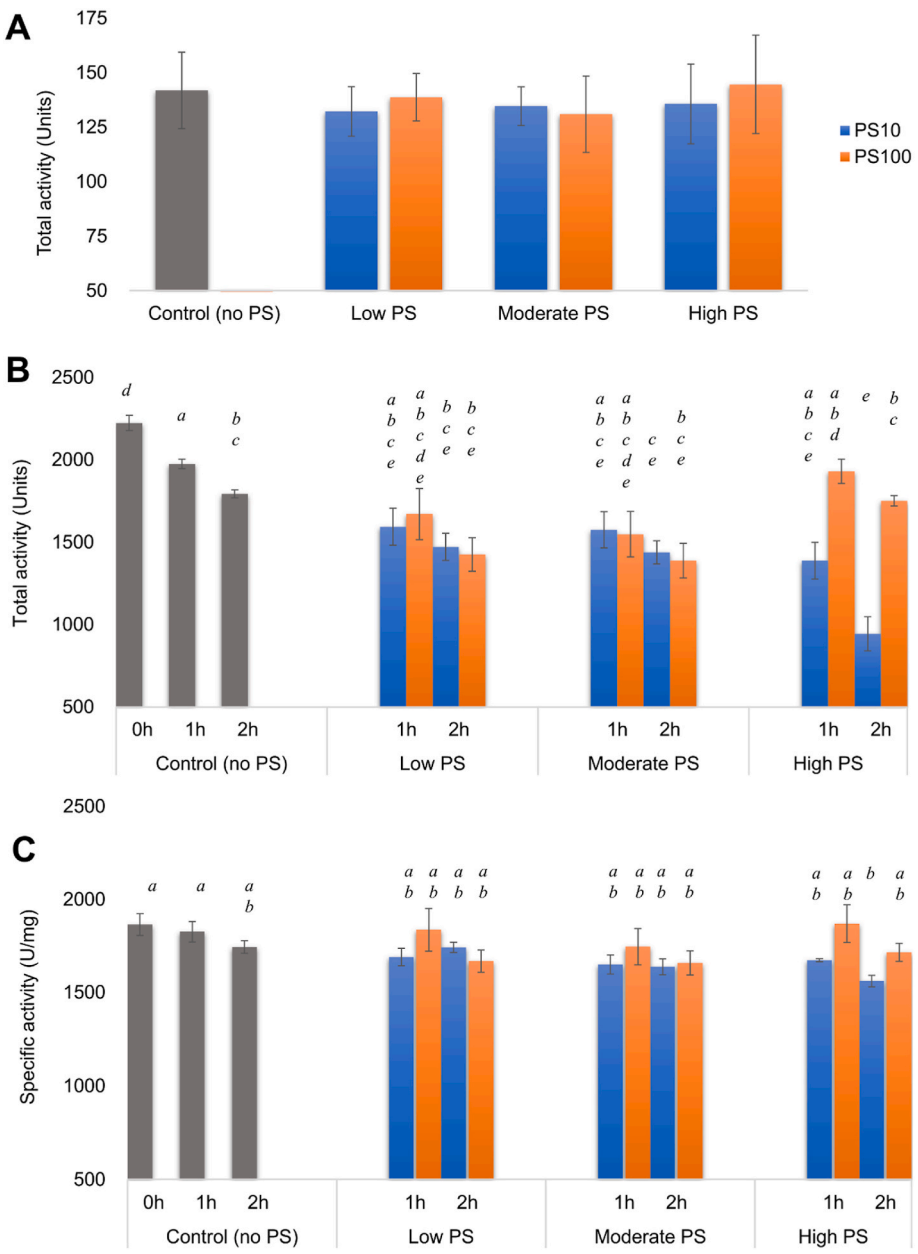

Fig. 2. Changes in (A) total activity during the quick 10 min exposure to PS, (B) total activity and (C) specific activity after 1h and 2h exposure to increasing concentrations of PS. Note that PS beads were kept in the pepsin solution in (A). On the contrary, PS were removed from the pepsin solution in (B) and (C); Letters indicate statistical significance at $p < 0.05$.

pepsin from the surface of PS may have occurred upon the addition of Hb, which had a 4x higher concentration (15.6 μg/mL vs 3.9 μg/mL).

In the second approach, the exposure time was prolonged to 1h and 2h, and PS particles were removed from the pepsin solution prior to the addition of Hb. The total activity of the control remarkably decreased with time (Fig. 2B). The lowest total activity was observed after 2h exposure to high PS10 ($p < 0.05$). The specific activity of pepsin exposed to high PS10 for 2h was also notably lower ($p < 0.05$) than that of the controls at 0h and 1h (Fig. 2C).

Pepsin exposed to PS100 for 2h yielded comparable enzyme activities to the controls, while 2h exposure to high PS10 consistently led to the inhibition of pepsin (Figure B and C). The soluble pepsin concentration decreased after 1h and 2h exposure to PS (Fig. S1). At 2h, the least protein concentration was observed in high PS10, with approximately 50% and 40% of pepsin significantly lost ($p < 0.05$) relative to the 0h and 2h controls, respectively, due to protein denaturation and adsorption on the PS beads.

3.3. Binding of pepsin to PS

The adsorption of pepsin on PS was fitted using four adsorption models: Langmuir, Freundlich, Redlich–Peterson (RP) and Guggenheim–Anderson–de Boer (GAB) as described in Section S7 of SI (Majd et al., 2022). According to adsorption equilibrium data (Fig. S2), better correlation coefficients were obtained for PS10 compared to PS100 for all tested adsorption models as shown in Table 1. The results showed that pepsin had a higher affinity for PS10 than for PS100, as indicated by K_L (Langmuir constant), K_r (Redlich–Peterson constant) and $K_{hard\ G}$ (adsorption constant for the hard corona), which are measures of pepsin affinity toward PS MPs. High ratio of $K_{hard\ G}/K_{soft\ G}$, which signifies adsorption from soft corona to hard corona, was about four times higher for PS10. This suggests much lower desorption of

Table 1
Langmuir, Freundlich, Redlich−Peterson and GAB isotherms constants for the adsorption of pepsin onto PS 10 and PS 100 MPs obtained by nonlinear regression analysis.

Isotherm model	Parameters	PS10 pH 3	PS100 pH 3
Langmuir	K_L (ml/mg)	2.836	1.264
	Q_L (mg/g)	456.95	485.32
	R_L	0.169	0.322
	R^2	0.942	0.681
Freundlich	K_F ((mg/g)*(L/mg)$^{1/n}$)	324.74	266.06
	N	2.865	2.160
	R^2	0.91	0.669
Redlich−Peterson	K_R (ml/mg)	1358	626
	α (ml/mg)	3.58	1.47
	β	0.976	0.983
	R^2	0.928	0.575
Guggenheim−Anderson−de Boer	Q_G (mg/g)	408.05	331.64
	K_{hard} G (ml/mg)	3.438	2.246
	$K_{soft\ G}$ (ml/mg)	0.045	0.112
	R^2	0.929	0.579

pepsin molecules from hard corona to soft corona in PS10 compared to PS100 due to stronger pepsin binding in the hard corona of PS10.

Furthermore, the adsorption capacity of PS MPs for pepsin was evaluated using Q_L (maximum amount of adsorbed protein), K_F (Freundlich constant, adsorption capacity), and Q_G (surface concentration of strongly adsorbed protein). According to K_F and Q_G, PS100 had about 20% lower capacity than PS10. The adsorption occurred at heterogeneous sites based on Freundlich isotherm since N values were higher than 1 for both PS10 and PS100. Heterogenicity was higher for PS10 than PS100 which is most likely due to multilayer adsorptions. Values $1<N<10$ indicate that pepsin was favorably adsorbed by both PS MPs, but adsorption was not linear, e.g., there was decreased interaction between PS and pepsin with the increase in pepsin density on MPs surface.

In RP isotherm, β values were close to 1 for both PS MPs, suggesting that experimental isotherms are approaching Langmuir more than Freundlich. The calculated R_L values (Langmuir equilibrium parameter) were $0 < R_L < 1$ for both tested MPs which implies that adsorption was favorable.

3.4. Changes in pepsin structure

To acquire insights on the structural changes of pepsin after incubation in SGF for 1h and 2h, with and without PS, far and near UV CD spectra, and Trp intrinsic fluorescence spectra of pepsin were recorded in solution after removal of PS particles. In this case, we used a pepsin:PS mass ratio of 1:1 (685 μg/mL of pepsin and PS) which is 8 times lower than pepsin:high PS10 mass ratio in Section 3.2 in order to perform better inspection of pepsin conformation changes.

The far UV CD spectra of pepsin alone (Fig. 3A, solid curves) showed a gradual increase in β-sheet on account of decrease in α-helix and random coil (Table 2). The α-helix/β-sheet ratio also decreased with time. When PS10 was present, differences were observed in the secondary structure content compared to native pepsin at all times (Fig. 3A, dotted curves), with a slight decrease in β-sheet and an increase in α-helix and random coil (Table 2).The α-helix/β-sheet ratio increased immediately after the addition of PS10 and continued to increase with time, which was opposite to the decreasing trend in pepsin alone. At 2h, the ratio with PS10 was 50% higher than pepsin without PS, indicating that pepsin adopted different conformations.

Pepsin alone showed decreased signal up to 295 nm with a weakened Trp peak at 290 nm, indicating a loosened tertiary structure with aromatic residues less fixed within the asymmetric environment (Fig. 3C, solid curves). However, PS10 led to an increase in signal at 260 nm and a drastic increase in Trp peak at 290 nm (Fig. 3C, dotted lines), implying stabilization and rigidification of the tertiary structure of pepsin by PS10.

A decrease in intrinsic Trp fluorescence can be observed for pepsin without PS (Fig. 3E, solid curves) as conformational changes shielded Trp residues from the aqueous phase. With PS10, Trp residues were already slightly shielded at 0h and remained shielded after 1h and 2h, confirming rigidification of tertiary structure by PS10 (Fig. 3E, dotted curves).

PS100 showed minimal changes in pepsin's secondary and tertiary structure with time, maintaining stability of the structure without the additional rigidification observed with PS10 (Fig. 3B, D, and F). According to fluorescence spectroscopy, after 2h, Trp residues were exposed to solvent as in native pepsin (Fig. 3F). This implies that PS100 stabilized pepsin's native-like secondary structure and maintained rigidity while preventing loosening of the tertiary structure.

Pepsin has a relatively high content of aromatic residues, with 10.7% compared to the 8.2% average in proteins (Prilusky et al., 2011). Trp intrinsic fluorescence suggests that a high portion of these residues are not buried, with λmax^{EM} for native pepsin at 350 nm (Fig. 3E). In general, Trp λmax^{EM} correlates with the degree of solvent exposure of the chromophore, ranging from 308 nm to 355 nm for buried and fully exposed Trp, respectively (Vivian and Callis, 2001).

3.5. Effect of PS10 on the gastric digestion of milk proteins

To study the impact of pepsin-MPs binding on the digestion of complex food samples, we simulated the gastric digestion of cow's milk in the presence of high PS10. This treatment was chosen since the lowest total and specific activities were observed after 2h exposure to high PS10. Milk proteins remained stable throughout the digestion process (Fig. S3A) and were quickly broken down into lower molecular weight peptides in PM (Fig. 4A). Caseins were completely digested within the first minutes, while beta-lactoglobulin, a protein known for its resistance to pepsin digestion, remained intact at 18 kDa (Reddy et al., 1988).

Most of the digestion products in PM were concentrated within the 10–35 kDa region of the gel. There was no drastic change in band thickness during the first 20 min, but a decline was observed from 30 min onwards. With PS10 (PMPS1), the pattern of digestion products was similar to PM as shown in Fig. 4B, but the total relative density at 10–35 kDa was slightly higher for 5–20 min and 30–120 min (Table 3). There was also a slight increase in total relative density of 2–9 kDa fragments.

In PMPS2, where PS10 increased from 3.9E-03 mg/mL to 0.3 mg/mL, the digestion products were similar to PMPS1 (Fig. 4C). However, total relative density increased even more for 10–35 kDa 2–9 kDa fragments (Table 3). This suggests that PS10 leads to accumulation of larger peptide fragments during the first minutes of digestion even though intact caseins were rapidly digested. A similar pattern of digestion products was observed regardless of the presence of PS and the delay in breakdown of larger peptides was more pronounced.

3.6. Formation of protein coronas

PS10 beads from PMPS2 were analyzed to examine the proteins/peptides bound to the surface during digestion. SDS-PAGE analysis revealed the formation of a soft corona and a hard corona consisting of loosely and strongly bound proteins, respectively. In the soft corona of pepsin alone, faint bands are present at 10 min and 15 min (Fig. 4D) and more pronounced bands can be observed in the hard corona at 5 min and from 20 min onwards (Fig. 4F). This suggests that unstable hard corona forms within first the 5 min which desorbs to the soft corona at 10 and 15 min. Finally, from 20 min, a stable hard corona was formed which remained until the end of digestion.

With milk, soft corona was not observed (Fig. 4E) while abundant hard corona was visible at 15 min (Fig. 4G). LC-MS/MS analyses (Section S8) revealed that majority of the prominent peptide bands on the hard corona (Fig. S4A) during the first 15 min of digestion came from

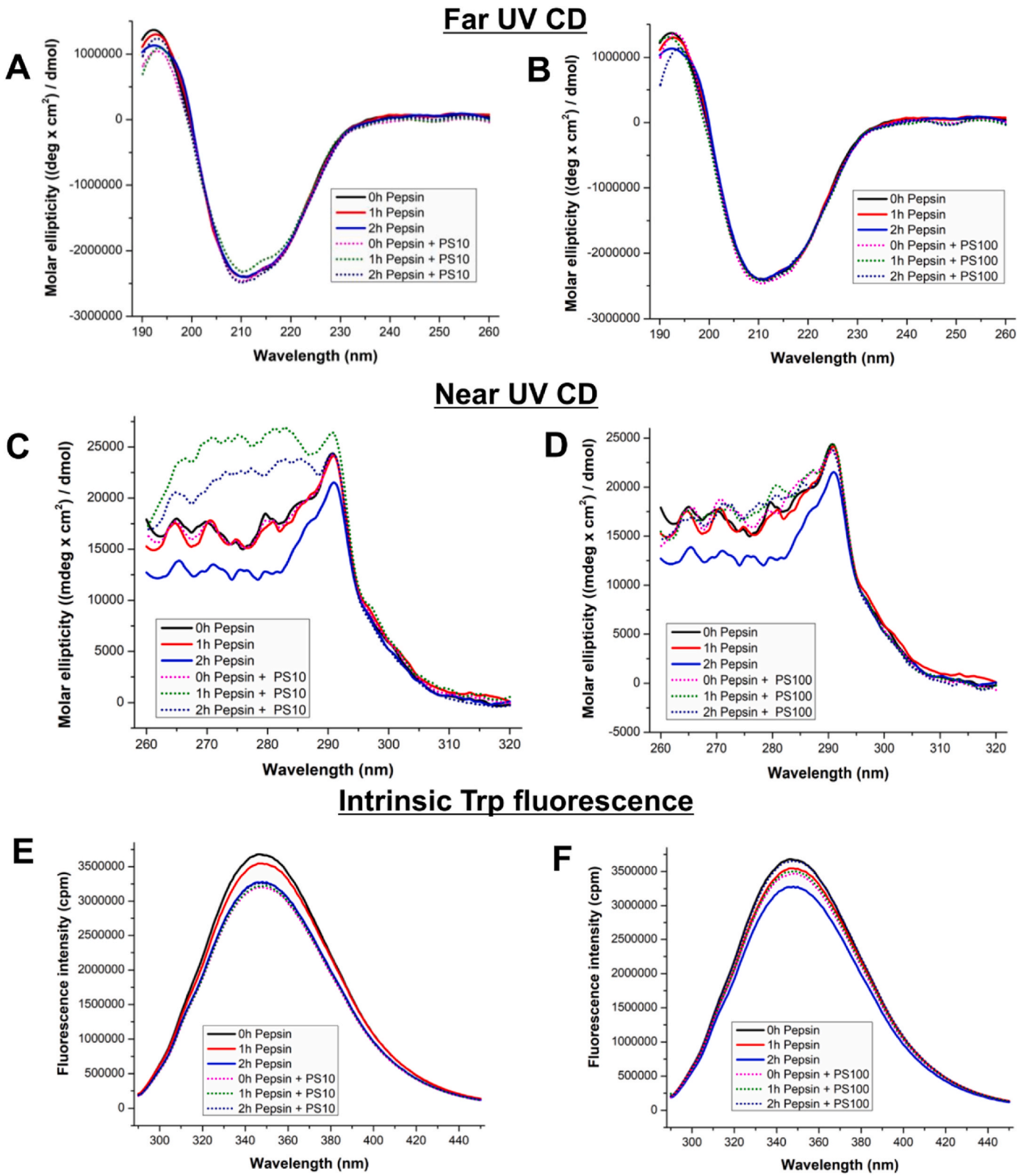

Fig. 3. Changes in pepsin secondary and tertiary structure after 1h and 2h exposure to PS (broken lines). Controls without PS are shown as solid lines; Far UV CD spectra for (A) PS10 and (B) PS100, near UV spectra for (C) PS10 and (D) PS100, and intrinsic tryptophan fluorescence (280 nm excitation) for (E) PS10 and (F) PS100.

Table 2
Estimated secondary structure content of pepsin.

Incubation time (hours)	α-helix (%)	β-sheet (%)	β-turn (%)	Random (%)	α-helix/ β-sheet ratio
Pepsin in SGF					
0	9.2	32.7	24.7	33.4	0.281
1	9.2	36.7	22.7	31.6	0.251
2	8.0	37.3	24.0	30.7	0.214
Pepsin in SGF with PS10					
0	10.1	32.0	23.3	34.6	0.316
1	9.9	32.1	23.7	34.2	0.308
2	10.2	31.7	23.4	34.7	0.322
Pepsin in SGF with PS100					
0	10.4	34.4	23.3	32.0	0.301
1	8.8	32.9	24.9	33.4	0.267
2	9.4	32.8	22.4	35.4	0.286

caseins (Fig. S4B and Table S4). After 10 and 15 min, fragments (<17 kDa) of caseins were present in the hard corona even though they could not be seen in solution of PMPS2 (Fig. 4C), while from 20 min until the end of digestion, only faint pepsin band was visible. This means protein fragments are bound to PS10 only during the existence of unstable pepsin hard corona. After its stabilization, the fragments are almost completely excluded due to Vroman effect (Hirsh et al., 2013).

4. Discussion

Despite the importance of ingestion exposure route and extensive documentation on sources and types of food contaminated with MPs, there is still limited information regarding its behavior and interaction with the human GIT. With the limited bioavailability of MPs, the highest exposure concentrations that will most likely cause potential health effects occur in the GIT (Ramsperger et al., 2022). We particularly focused on small size PS (10 μm) due to high potential exposure to 1–10 μm MP. It has been shown that apples contain 2.23E+05 particles/g of small MPs (Oliveri Conti et al., 2020). With the intake of only one apple (cca 100 g) for every 250 mL gastric fluid in adults (Mudie et al., 2014) or 25 mL of gastric fluid in children (Van der Veken et al., 2022), transient concentration of small size MPs can result in around 9.2E+02 to 9.2E+03 particles/mL. This transient peak concentrations upon ingestion of food contaminated with high number of MPs were mimicked in our study. We also investigated lower exposure level of MPs, such as 2.2E+02 particles/mL, that could be more relevant for foods containing larger MPs (50–250 μm) and less MP particles/individual such as seafood (World Health Organization, 2022).

Quick exposure to PS10 or PS100 (1st format of the activity assay, Fig. 2A) did not affect enzyme performance which suggests that only a minimal amount of pepsin interacted with PS followed by its quick displacement by the more abundant Hb substrate. Despite the unremarkable differences, activity with PS100 was slightly higher than PS10 due to stronger interaction between PS100 and Hb. At pH 2, Hb is positively charged (pI = 6.9) which makes it electrostatically attracted to the more negative PS100 (Fig. 1D). This led to minimized pepsin-PS100 interaction and better enzyme performance. It is also interesting to note that exposure to high PS100 yielded slightly higher activity ($p > 0.05$) than the control (Fig. 2A). This was most likely due to PS100-induced conformational changes in Hb which made it more susceptible to peptic cleavage.

When exposure to PS10 or PS100 was prolonged (2nd format of the activity assay), specific activity remarkably decreased only for PS10, even though for the same number of particles, PS100 had 100 times larger surface area and 1000 times higher mass than PS10 for the same number of particles. As long exposure to PS is expected to occur in reality based on the time of gastric retention, negative effect on enzyme activity is not entirely inconceivable; but surprisingly, it was only observed in PS10. This is once again a consequence of the pronounced negative charge of PS100 compared to PS10 (Fig. 1D). Since pepsin has a pI of 2.76–2.90 (Lee et al., 2020), it has a negative charge in pH 3 SGF. Therefore, there was greater repulsion between pepsin and PS100, reducing their tendency to interact and inactivate pepsin. In the absence of abundant protein substrate (Hb), pepsin binds to PS and affinity constants calculated for PS10 are higher than for PS100 (Table 1). Although the PS beads used in this study were unmodified and non-functionalized according to the manufacturer, charged groups were still present on top of the hydrophobic backbone and aromatic phenyl group, resulting in a measurable negative zeta potential. Sulfate groups are highly likely to be present on the beads since general synthesis of PS involves the use of potassium persulfate as initiator. This leaves terminal sulfate groups at the surface of the particles which gives a net negative surface charge (Al-Sid-Cheikh et al., 2020).

The binding interaction between pepsin and PS (Table 1 and Fig. S2) show higher binding constant between PS10 and pepsin. Although our experimental system (adsorption of proteins to plastic microparticles) does not meet any of Langmuir assumptions (monolayer adsorption, homogeneous sites, constant adsorption energy and no lateral interaction between the adsorbed molecules)(Majd et al., 2022), this model can provide at least a rough estimation of adsorption affinity and capacity (Table 1). However, Langmuir isotherm cannot discriminate adsorption capacity between PS10 and PS100 compared to Freundlich and GAB models. In general, for protein adsorption on micro/nanoparticles (NPs), GAB model seems to be the most relevant (Meissner et al., 2015; J. G. Lee et al., 2020) providing additional $K_{soft\ G}$ constant describing adsorption and desorption between soft corona and bulk solution.

Protein adsorption on MPs and NPs depend on the type of plastics, protein sequence and conformation, particle size, particle surface, as well as conditions in solution such as pH, ionic strength, and temperature. In our study, PS10 and PS100 differ only in surface per mass unit and surface charge per surface unit. This explains why PS10 and PS100 differ in adsorption capacity and affinity in all models. The surface area of PS10 is ten times higher than that of the same mass of PS100, resulting in lower adsorption capacity. The difference in adsorption affinity can be explained by the greater repulsion between pepsin and PS100. Even though pepsin have few basic residues (Arg307, Arg315, and Lys319) whose positive charge may contribute to electrostatic interaction, these residues engage in the formation of ion pairs, thereby making it unlikely to be involved in the interaction with PS (Andreeva et al., 1981). However, adsorption of pepsin in soft corona ($K_{soft\ G}$) is higher in PS100, implying that protein to protein adsorption, e.g., protein – protein binding is stronger in PS100, in comparison to PS10.

The hydrophobic interaction between the aromatic side chains of PS and aromatic residues of pepsin, which includes 14 Phe, 5 Trp, and 16 Tyr (Bateman et al., 2021), play an important role in PS-pepsin binding. In a study by Zhang and Casabianca (2018), it was shown that electrostatic and hydrophobic interactions of long-chain aliphatic amino acids lead to relatively weak binding, while aromatic amino acids exhibit comparatively much stronger binding to negatively-charged PS NPs, indicating π−π interactions between the aromatic side chain of the amino acid and the phenyl rings in PS.

As discussed in Section S9 of SI, 20 of the 35 aromatic residues in pepsin are not buried which makes them available for interaction with the phenyl side chains of P S (Fig. S5 and Table S5). In pepsin, Trp λ_{max} is 347 nm, suggesting that tryptophans are mostly solvent exposed. This means that in the folded conformation, tryptophans are involved in π−π interactions with phenol rings of PS while other hydrophobic interactions contribute to a lesser extent. However, upon more extensive unfolding of pepsin, PS hydrophobic interactions with buried aliphatic and aromatic residues become significant.

This hydrophobic interaction through the backbone and aromatic side chain of PS was favored by the high ionic strength of SGF- it weakened the negative charge of (1) PS sulfate groups and (2) deprotonated pepsin carboxyl group, thus reducing repulsion, and (3) suppressed eventual electrostatic interactions of polar residues with the PS

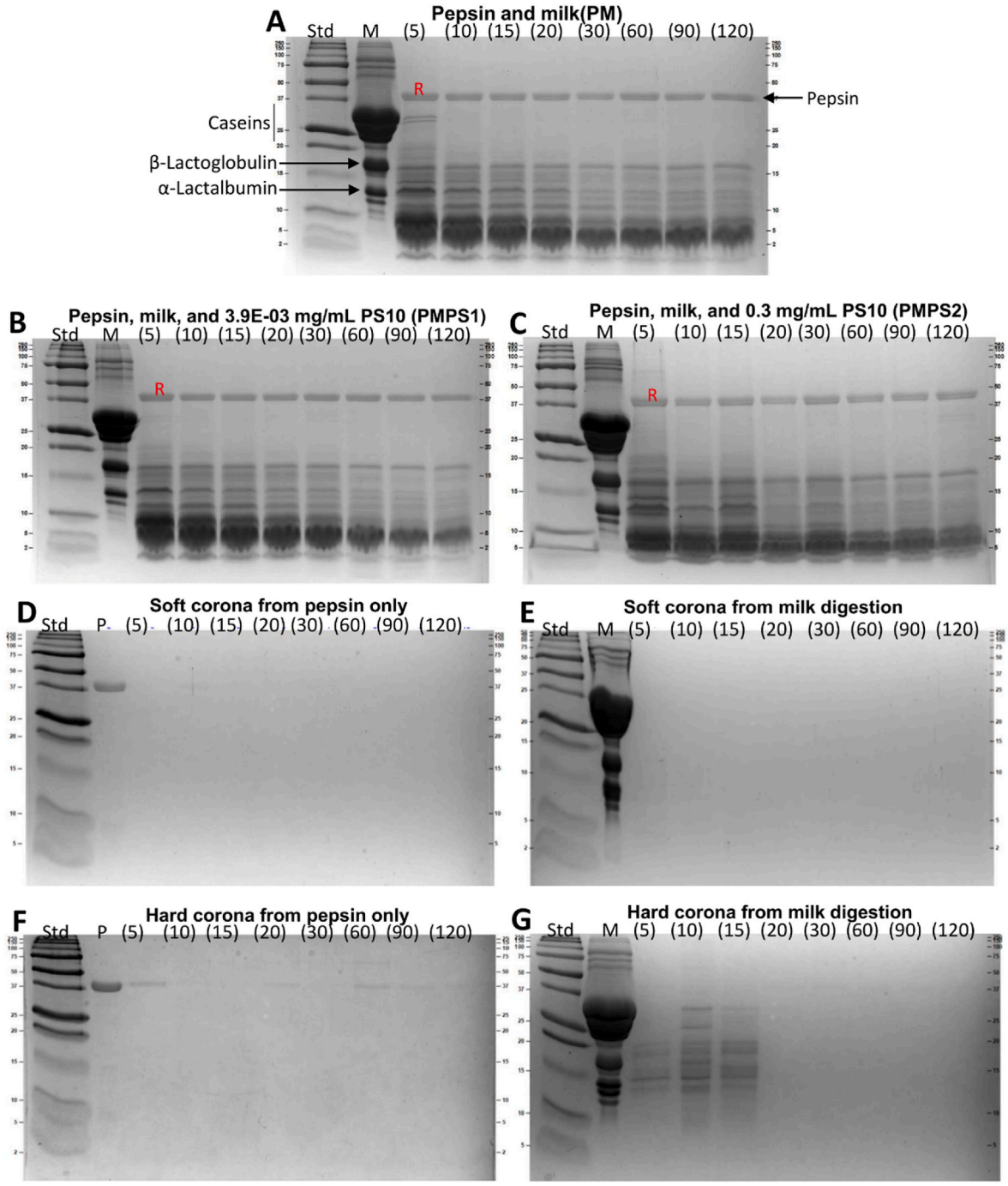

Fig. 4. Polyacrylamide gels showing gastric digestion products from (A) PM- Pepsin and milk, (B) PMPS1- Pepsin, milk, and 3.9E-03 mg/mL PS10, and (C) PMPS2- Pepsin, milk, and 0.30 mg/mL PS10; Soft protein corona extracted from the beads after *in vitro* simulated gastric digestion involving (D) pepsin only and (E) pepsin with milk; Hard protein corona extracted from the beads after *in vitro* simulated gastric digestion involving (F) pepsin only and (G) pepsin with milk; Numbers on top of the gels indicate the timepoint of gastric digestion; R signifies the band used as reference for the calculation of rel. den.; M is cow's milk only; P is pepsin only.

sulfate group which further stimulated hydrophobic interactions.

The loss of specific activity after being separated from PS (2nd format of pepsin activity) suggests more profound effects on the protein conformation and functionality as observed in CD and fluorescence spectroscopy. After prolonged exposure to PS10, the soluble pepsin fraction showed an increased α-helix/β-sheet ratio (Table 2) which indicates a conformational change where structure becomes more rigid, opposite to the changes that occurred in pepsin alone (incubated for the same time in SGF). Increase in the Trp characteristic peak (Fig. 3C) could signify Trp residues becoming more anchored to the asymmetric environment. Decline in intrinsic Trp fluorescence (Fig. 3E) also indicates a shielding effect brought by the stiffening of the structure. These changes could not be observed on the enzyme exposed to PS100 (Fig. 3D and F, and Table S4). There was a slight change in conformation but no additional rigidification occurred because of the lower binding affinity brought about by the more negative zeta potential of PS100 (Fig. 1D).

Even though a high degree of secondary and tertiary structure was retained after 2h for pepsin with PS10 and pepsin alone, the necessary conformation for the enzyme to stay active was not maintained. In its native conformation, pepsin's active site is located in between its two

Table 3
Total relative density of peptide bands. PM- Pepsin and milk; PMPS1- Pepsin, milk, and 3.9E-03 mg/mL PS10; PMPS2- Pepsin, milk, and 0.30 mg/mL PS10.

Sample	Total relative density			
	10–35 kDa peptides		2–9 kDa peptides	
	5–20 min	30–120 min	5–20 min	30–120 min
PM	8.69 ± 2.29	3.33 ± 0.38	55.76 ± 0.17	35.91 ± 1.25
PMPS1	10.93 ± 0.72	6.43 ± 2.23	55.95 ± 2.59	42.13 ± 4.23
PMPS2	12.06 ± 1.18	9.44 ± 2.46	44.90 ± 12.90	41.02 ± 12.75
Fold-change				
PMPS1/PM	1.26	1.93	1.00	1.17
PMPS2/PM	1.39	2.83	0.81	1.14

domains where each domain holds a catalytic aspartic acid residue (Asp32 and Asp215). As such, proper conformation of both domains is crucial in preserving the active site cleft (Dee et al., 2006). The relatively rigid or loose pepsin structure increasingly dominated the soluble phase as the incubation progressed. However, the inhibition cannot be considered as solely a consequence of structural changes. The physical removal of pepsin due to adsorption on PS also slightly contributed. Autolysis or autodigestion of proteolytic enzymes is also another factor to consider. Pepsin autolysis is a known phenomenon where pepsin digests itself leading to peptide bond hydrolysis and specific activity decay (Perlmann, 1954; Qiao et al., 2002). The rate of autolysis is higher at lower pH values (e.g., pH 2 vs pH 4) and low protein concentrations, which are similar to the conditions of the PS-pepsin exposure experiment in this study.

Cow's milk proteins were rapidly digested by pepsin, particularly the most abundant proteins, caseins. In the presence of PS10, the pattern of protein digestion was not affected. Digestion of caseins also proceeded rapidly in the presence of PS10. However, the increased fold-change of 10–35 kDa fragments in the presence of PS10 suggests accumulation of larger polypeptides (Table 3). The effect was more pronounced with the higher concentration of MPs added to the digestion mixture (Fig. 4C and Table 3). As no significant inhibition of digestion was observed, it seems that proteins from the milk intervened or shielded pepsin from the potential loss of activity since they were more abundant (7.5 mg/mL) than pepsin (0.685 mg/mL).

In a multi-protein system, more abundant proteins adhere first to the particle surface in a very short time to form dynamic entities, and then are replaced by proteins with higher affinity to form stable entities (Yu et al., 2022). Corona formation in a dynamic multi-component system, such as digestive tract, is probably even more complex. Analysis of hard and soft corona during 2h digestion demonstrated that stable pepsin hard corona is formed after 20 min (Fig. 4F), and that milk protein fragments/peptides are bound to PS10 (Fig. 4G) only during existence of unstable pepsin hard corona. After its stabilization, protein fragments are almost completely excluded from hard corona due to Vroman effect. Therefore, digestion proceeds even with proteins bound in the hard corona but with important consequences on the survival of larger polypeptides/intact proteins for a longer period than in the case of digestion without the presence of MPs.

Interestingly, the most abundant protein identified in the hard corona was α_{S2}-casein (Fig. S4 and Table S4).This protein is just a minor fraction of milk proteins, making up only 9–10% of the total caseins in cow's milk and only around 20% of all α_S-caseins (Farkye and Shah, 2014), but it became enriched in the hard corona. Furthermore, the fragments of the α_{S2}-casein bound in hard corona span the C-terminal part of the protein, known for its hydrophobicity, susceptibility to fibril formation under physiological conditions (Thorn et al., 2008), and harboring epitopes (AA 171–180 on α_{S2}-casein) relevant in persistent cow's milk allergy (Järvinen et al., 2002). This may present serious health implications as the epitopes are carried during realistic gastric emptying process. On the other hand, it could also reduce the availability of these allergens and minimize their potential interaction with immune system components.

In a study by Tan et al. (2020), exposure to PS MPs resulted in reduced lipid digestion by gastric lipases. PS also altered the native structure of lipase which led to a decline in its activity, similar to what was observed in this study. Lipids and lipases were also found to bind to PS which is parallel to the adsorption of pepsin and milk proteins. An important observation that stems from our study is the impact of surface chemistry of MPs on their biological effects in the GIT. Aged MPs may exhibit quite different biological effects than manufactured particles commonly used for *in vitro* testing.

The reduced gastric breakdown of milk proteins in the presence of small size PS could potentially create complications on downstream nutrient assimilation. Protein hydrolysis by pepsin is a critical part of food disintegration during the gastric phase (Guo et al., 2020). Trypsin and chymotrypsin will further hydrolyze the peptides in the intestine, but the reduced fraction of short peptides in the stomach already limits the bioavailability of nutrients being fed downstream.

The static *in vitro* gastric model used in the study has limitations especially in terms of gastrointestinal passage. As such, this model does not mimic the natural emptying of the gut. The constant gut emptying process may allow the PS MPs, and the proteins bound to it, to reach the lower GIT which could provide different repertoire of peptides and epitopes of allergenic proteins. This deserves further investigation through *in vitro* dynamic multi-compartmental models coupled or not to cellular cultures, 3D models like intestinal organoids, and gut-on-a-chip microfluidic devices (Fournier et al., 2021). Furthermore, the static digestion model does not emulate the conditions of people suffering from digestive disorders such as enzyme deficiency. Despite these limitations, this is the first study demonstrating that pepsin, as well as its protein substrates, absorb to MPs leading to enzyme inhibition and altered protein digestion.

According to the results of this study, the presence of MPs in GIT of adults will hardly cause any significant effect on protein digestibility, considering that the relevant effects are only seen during digestion of real food with very high concentrations of MPs. The approach used in our study may open path for the further research, particularly on the effects of nanoplastics, able to pass cell membranes and blood-brain barrier (Shan et al., 2022), on proteins whose structural changes are directly related to autoimmune diseases, prion diseases, neurological and neurodegenerative diseases such as Alzheimer's or Parkinson's.

5. Conclusion

This study provides in-depth investigation of the impacts of PS MPs on pepsin and protein gastric digestion in physiologically relevant conditions (simulated gastric environment). To the best of our knowledge, this is the first study that describes the kinetics of *in vitro* gastric digestion of actual food proteins in the presence of PS MPs. We found that binding forces between pepsin and MP, which are predominantly dictated by surface chemistry, direct its biological activity or enzymatic action. Small size, practically uncharged PS, reduced pepsin activity with the following mechanism: (1) binding of pepsin to PS in hard corona due to hydrophobic interactions between phenyl groups and aromatic amino acid residues, and (2) gradual changes in bulk enzyme structure forming rigid, non-natively folded conformation. In the presence of food proteins, small MPs preferentially bind cow's milk proteins and pepsin. Digestion in the presence of small PS led to a transient accumulation of larger peptides of cow's milk proteins (10–35 kDa) in the digestion mixture, as well as reduced bioavailability of short peptides (2–9 kDa) in the gastric phase.

The focus of this study was on monodispersed PS MPs of a well-defined size, but MPs found in food are mixed, variable, and polydispersed. Nevertheless, this work presents valuable insights regarding the interaction of PS MPs, food proteins, and pepsin, and their dynamics during gastric digestion which provides new knowledge and understanding on the potential risks of MPs to human health.

Author contribution statement

Maria Krishna de Guzman: Investigation, Data curation, Methodology, Formal analysis, Validation, Visualization, Writing – original draft, Writing – review & editing. Dragana Stanic-Vucinic: Investigation, Formal analysis, Writing – original draft, Writing – review & editing. Nikola Gligorijevic: Methodology, Investigation, Formal analysis. Lukas Wimmer: Methodology, Investigation. Manvel Gasparyan: Methodology, Writing – review & editing. Tamara Vasovic: Methodology, Formal analysis. Tamara Lujic - Formal analysis, Writing – review & editing. Lea Ann Dailey: Writing – review & editing. Sam Van Haute: Supervision, Writing – review & editing. Tanja Cirkovic Velickovic: Conceptualization, Methodology, Supervision, Funding acquisition, Project administration, Resources, Writing – review & editing.

Declaration of competing interest

The authors declare that they have no known competing financial interests or personal relationships that could have appeared to influence the work reported in this paper.

Data availability

Data will be made available on request.

Acknowledgement

This study was supported by the Ghent University Global Campus; Special Research Fund (BOF) of Ghent University (grant number 01N01718); and IMPTOX European Union's Horizon 2020 research and innovation program (grant number 965173). This research was also supported by the Serbian Academy of Sciences and Arts (grant number F-26) and the Ministry of Science, Innovation and technological development of the Republic of Serbia (Contract number: 451-03-68/2022-14/200168).

Appendix A. Supplementary data

Supplementary data related to this article can be found at https://doi.org/10.1016/j.envpol.2023.122282.

References

Al-Sid-Cheikh, M., Rowland, S.J., Kaegi, R., Henry, T.B., Cormier, M.A., Thompson, R.C., 2020. Synthesis of 14C-labelled polystyrene nanoplastics for environmental studies. Commun. Mater. 1, 1–8. https://doi.org/10.1038/s43246-020-00097-9.

Andreeva, N.S., Zdanov, A.A., Fedorov, A.A., 1981. Arrangement of the charged groups in the three-dimensional structure of pepsin. FEBS Lett 125, 239–241.

Anson, M.L., Mirsky, A.E., 1932. The estimation of pepsin with hemoglobin. J. Gen. Physiol. 16, 59.

Bateman, A., Martin, M.J., Orchard, S., Magrane, M., Agivetova, R., Ahmad, S., Alpi, E., Bowler-Barnett, E.H., Britto, R., Bursteinas, B., Bye-A-Jee, H., Coetzee, R., Cukura, A., da Silva, A., Denny, P., Dogan, T., Ebenezer, T.G., Fan, J., Castro, L.G., Garmiri, P., Georghiou, G., Gonzales, L., Hatton-Ellis, E., Hussein, A., Ignatchenko, A., Insana, G., Ishtiaq, R., Jokinen, P., Joshi, V., Jyothi, D., Lock, A., Lopez, R., Luciani, A., Luo, J., Lussi, Y., MacDougall, A., Madeira, F., Mahmoudy, M., Menchi, M., Mishra, A., Moulang, K., Nightingale, A., Oliveira, C.S., Pundir, S., Qi, G., Raj, S., Rice, D., Lopez, M.R., Saidi, R., Sampson, J., Sawford, T., Speretta, E., Turner, E., Tyagi, N., Vasudev, P., Volynkin, V., Warner, K., Watkins, X., Zaru, R., Zellner, H., Bridge, A., Poux, S., Redaschi, N., Aimo, L., Argoud-Puy, G., Auchincloss, A., Axelsen, K., Bansal, P., Baratin, D., Blatter, M.C., Bolleman, J., Boutet, E., Breuza, L., Casals-Casas, C., de Castro, E., Echioukh, K.C., Coudert, E., Cuche, B., Doche, M., Dornevil, D., Estreicher, A., Famiglietti, M.L., Feuermann, M., Gasteiger, E., Gehant, S., Gerritsen, V., Gos, A., Gruaz-Gumowski, N., Hinz, U., Hulo, C., Hyka-Nouspikel, N., Jungo, F., Keller, G., Kerhornou, A., Lara, V., Le Mercier, P., Lieberherr, D., Lombardot, T., Martin, X., Masson, P., Morgat, A., Neto, T.B., Paesano, S., Pedruzzi, I., Pilbout, S., Pourcel, L., Pozzato, M., Pruess, M., Rivoire, C., Sigrist, C., Sonesson, K., Stutz, A., Sundaram, S., Tognolli, M., Verbregue, L., Wu, C.H., Arighi, C.N., Arminski, L., Chen, C., Chen, Y., Garavelli, J.S., Huang, H., Laiho, K., McGarvey, P., Natale, D.A., Ross, K., Vinayaka, C.R., Wang, Q., Wang, Y., Yeh, L.S., Zhang, J., Ruch, P., Teodoro, D., 2021. UniProt: the universal protein knowledgebase in 2021. Nucleic Acids Res. 49, D480–D489. https://doi.org/10.1093/nar/gkaa1100.

Brodkorb, A., Egger, L., Alminger, M., Alvito, P., Assunção, R., Ballance, S., Bohn, T., Bourlieu-Lacanal, C., Boutrou, R., Carrière, F., others, 2019. INFOGEST static in vitro simulation of gastrointestinal food digestion. Nat. Protoc. 14, 991–1014.

Chanpiwat, P., Damrongsiri, S., 2021. Abundance and characteristics of microplastics in freshwater and treated tap water in Bangkok, Thailand. Environ. Monit. Assess. 193, 1–15. https://doi.org/10.1007/S10661-021-09012-2/FIGURES/6.

Clogston, J.D., Patri, A.K., 2011. Zeta potential measurement. Charact. nanoparticles Intend. drug Deliv. 63–70.

Cox, K.D., Covernton, G.A., Davies, H.L., Dower, J.F., Juanes, F., Dudas, S.E., 2019. Human consumption of microplastics. Environ. Sci. Technol. 53, 7068–7074.

de Guzman, M.K., Andjelković, M., Jovanović, V., Jung, J., Kim, J., Dailey, L.A., Rajković, A., De Meulenaer, B., Ćirković Veličković, T., 2022. Comparative profiling and exposure assessment of microplastics in differently sized Manila clams from South Korea by μFTIR and Nile Red staining. Mar. Pollut. Bull. 181, 113846 https://doi.org/10.1016/J.MARPOLBUL.2022.113846.

Dee, D., Pencer, J., Nieh, M.P., Krueger, S., Katsaras, J., Yada, R.Y., 2006. Comparison of solution structures and stabilities of native, partially unfolded and partially refolded pepsin. Biochemistry 45, 13982–13992. https://doi.org/10.1021/bi061270i.

Diaz-Basantes, M.F., Conesa, J.A., Fullana, A., 2020. Microplastics in honey, beer, milk and refreshments in Ecuador as emerging contaminants. Sustainability 12 (14), 5514. https://doi.org/10.3390/SU12145514.

Dong, X., Liu, X., Hou, Q., Wang, Z., 2023. From natural environment to animal tissues: a review of microplastics(nanoplastics) translocation and hazards studies. Sci. Total Environ. 855, 158686 https://doi.org/10.1016/j.scitotenv.2022.158686.

EFSA, 2016. Presence of microplastics and nanoplastics in food, with particular focus on seafood. EFSA J. 14, e04501 https://doi.org/10.2903/J.EFSA.2016.4501.

Erni-Cassola, G., Zadjelovic, V., Gibson, M.I., Christie-Oleza, J.A., 2019. Distribution of plastic polymer types in the marine environment; A meta-analysis. J. Hazard Mater. 369, 691–698. https://doi.org/10.1016/J.JHAZMAT.2019.02.067.

Farkye, N.Y., Shah, N., 2014. Milk proteins. In: Applied Food Protein Chemistry, pp. 427–458. https://doi.org/10.1002/9781118860588.ch16.

Fournier, E., Etienne-Mesmin, L., Grootaert, C., Jelsbak, L., Syberg, K., Blanquet-Diot, S., Mercier-Bonin, M., 2021. Microplastics in the human digestive environment: a focus on the potential and challenges facing in vitro gut model development. J. Hazard Mater. 415, 125632 https://doi.org/10.1016/j.jhazmat.2021.125632.

Galloway, T.S., 2015. Micro- and nano-plastics and human health. In: Marine Anthropogenic Litter, pp. 1–447. https://doi.org/10.1007/978-3-319-16510-3.

Gendel, S.M., Zhu, J., 2013. Analysis of U.S. Food and drug administration food allergen recalls after implementation of the food allergen labeling and consumer protection act. J. Food Prot. 76 (11), 1933–1938. https://doi.org/10.4315/0362-028X.JFP-13-171.

Goodsell, D.S., Dutta, S., Zardecki, C., Voigt, M., Berman, H.M., Burley, S.K., 2015. The RCSB PDB "molecule of the month": inspiring a molecular view of biology. PLoS Biol. 13, 1–12. https://doi.org/10.1371/journal.pbio.1002140.

Guo, Q., Ye, A., Singh, H., Rousseau, D., 2020. Destructuring and restructuring of foods during gastric digestion. Compr. Rev. Food Sci. Food Saf. 19, 1658–1679. https://doi.org/10.1111/1541-4337.12558.

Hernandez, L.M., Xu, E.G., Larsson, H.C.E., Tahara, R., Maisuria, V.B., Tufenkji, N., 2019. Plastic teabags release billions of microparticles and nanoparticles into tea. Environ. Sci. Technol. 53 (21), 12300–12310. https://doi.org/10.1021/acs.est.9b02540.

Hirsh, S.L., McKenzie, D.R., Nosworthy, N.J., Denman, J.A., Sezerman, O.U., Bilek, M.M. M., 2013. The Vroman effect: competitive protein exchange with dynamic multilayer protein aggregates. Colloids Surf., B 103, 395–404.

Hirt, N., Body-Malapel, M., 2020. Immunotoxicity and intestinal effects of nano-and microplastics: a review of the literature. Part. Fibre Toxicol. 17 https://doi.org/10.1186/s12989-020-00387-7.

Järvinen, K.-M., Beyer, K., Vila, L., Chatchatee, P., Busse, P.J., Sampson, H.A., 2002. B-cell epitopes as a screening instrument for persistent cow's milk allergy. J. Allergy Clin. Immunol. 110, 293–297. https://doi.org/10.1067/mai.2002.126080.

Jin, M., Wang, X., Ren, T., Wang, J., Shan, J., 2021. Microplastics Contamination in Food and Beverages: Direct Exposure to Humans. https://doi.org/10.1111/1750-3841.15802.

Kankanige, D., Babel, S., 2020. Smaller-sized micro-plastics (MPs) contamination in single-use PET-bottled water in Thailand. Sci. Total Environ. 717, 137232 https://doi.org/10.1016/J.SCITOTENV.2020.137232.

Lee, J.G., Lannigan, K., Shelton, W.A., Meissner, J., Bharti, B., 2020. Adsorption of myoglobin and corona formation on silica nanoparticles. Langmuir 36 (47), 14157–14165. https://doi.org/10.1021/acs.langmuir.0c01613.

Li, D., Shi, Y., Yang, L., Xiao, L., Kehoe, D.K., Gun'ko, Y.K., Boland, J.J., Wang, J.J., 2020. Microplastic release from the degradation of polypropylene feeding bottles during infant formula preparation. Nat. Food 1, 746–754. https://doi.org/10.1038/s43016-020-00171-y.

Majd, M.M., Kordzadeh-Kermani, V., Ghalandari, V., Askari, A., Sillanpää, M., 2022. Adsorption isotherm models: a comprehensive and systematic review (2010− 2020). Sci. Total Environ. 812, 151334.

Makhdoumi, P., Amin, A.A., Karimi, H., Pirsaheb, M., Kim, H., Hossini, H., 2021. Occurrence of microplastic particles in the most popular Iranian bottled mineral water brands and an assessment of human exposure. J. Water Process Eng. 39, 101708 https://doi.org/10.1016/J.JWPE.2020.101708.

Mason, S.A., Vg, W., Neratko, J., 2018. Synthetic polymer contamination in bottled water. Front. Chem. 6, 407. https://doi.org/10.3389/fchem.2018.00407.

Meissner, J., Prause, A., Bharti, B., Findenegg, G.H., 2015. Characterization of protein adsorption onto silica nanoparticles: influence of pH and ionic strength. Colloid Polym. Sci. 293, 3381–3391.

Mudie, D.M., Murray, K., Hoad, C.L., Pritchard, S.E., Garnett, M.C., Amidon, G.L., Gowland, P.A., Spiller, R.C., Amidon, G.E., Marciani, L., 2014. Quantification of

gastrointestinal liquid volumes and distribution following a 240 mL dose of water in the fasted state. Mol. Pharm. 11, 3039–3047.
Oliveri Conti, G., Ferrante, M., Banni, M., Favara, C., Nicolosi, I., Cristaldi, A., Fiore, M., Zuccarello, P., 2020. Micro- and nano-plastics in edible fruit and vegetables. The first diet risks assessment for the general population. Environ. Res. 187 https://doi.org/10.1016/J.ENVRES.2020.109677.
Perlmann, G.E., 1954. Formation of enzymatically active, dialysable fragments during autodigestion of pepsin. Nature 173, 406.
Pivokonsky, M., Cermakova, L., Novotna, K., Peer, P., Cajthaml, T., Janda, V., 2018. Occurrence of microplastics in raw and treated drinking water. Sci. Total Environ. 643, 1644–1651. https://doi.org/10.1016/j.scitotenv.2018.08.102.
Prata, J.C., Paço, A., Reis, V., da Costa, J.P., Fernandes, A.J.S., da Costa, F.M., Duarte, A. C., Rocha-Santos, T., 2020. Identification of microplastics in white wines capped with polyethylene stoppers using micro-Raman spectroscopy. Food Chem. 331, 127323 https://doi.org/10.1016/j.foodchem.2020.127323.
Prilusky, J., Hodis, E., Canner, D., Decatur, W.A., Oberholser, K., Martz, E., Berchanski, A., Harel, M., Sussman, J.L., 2011. Proteopedia: a status report on the collaborative, 3D web-encyclopedia of proteins and other biomolecules. J. Struct. Biol. 175, 244–252.
Qiao, Y., Gumperts, M., Kempen Van, T., 2002. Stability of pepsin (EC 3.4. 23.1) during in vitro protein digestibility assay 1, 2. J. Food Biochem. 26, 355–375.
Ramsperger, A.F.R.M., Bergamaschi, E., Panizzolo, M., Fenoglio, I., Barbero, F., Peters, R., Undas, A., Purker, S., Giese, B., Lalyer, C.R., 2022. Nano-and microplastics: a comprehensive review on their exposure routes, translocation, and fate in humans. NanoImpact, 100441.
Ranjan, V.P., Joseph, A., Goel, S., 2021. Microplastics and other harmful substances released from disposable paper cups into hot water. J. Hazard Mater. 404, 124118 https://doi.org/10.1016/j.jhazmat.2020.124118.
Reddy, I.M., Kella, N.K.D., Kinsella, J.E., 1988. Structural and conformational basis of the resistance of. beta.-lactoglobulin to peptic and chymotryptic digestion. J. Agric. Food Chem. 36, 737–741.
Schwabl, P., 2020. Microplastics in hot water. Nat. Food 1, 671–672. https://doi.org/10.1038/s43016-020-00174-9.
Shan, S., Zhang, Y., Zhao, H., Zeng, T., Zhao, X., 2022. Polystyrene nanoplastics penetrate across the blood-brain barrier and induce activation of microglia in the brain of mice. Chemosphere 298, 134261. https://doi.org/10.1016/j.chemosphere.2022.134261.
Shruti, V.C., Pérez-Guevara, F., Elizalde-Martínez, I., Kutralam-Muniasamy, G., 2020. First study of its kind on the microplastic contamination of soft drinks, cold tea and energy drinks - future research and environmental considerations. Sci. Total Environ. 726, 138580 https://doi.org/10.1016/j.scitotenv.2020.138580.
Tan, H., Yue, T., Xu, Y., Zhao, J., Xing, B., 2020. Microplastics reduce lipid digestion in simulated human gastrointestinal system. Environ. Sci. Technol. 54, 12285–12294. https://doi.org/10.1021/acs.est.0c02608.
Thorn, D.C., Ecroyd, H., Sunde, M., Poon, S., Carver, J.A., 2008. Amyloid fibril formation by bovine milk αs2-casein occurs under physiological conditions yet is prevented by its natural counterpart, αs1-casein. Biochemistry 47, 3926–3936. https://doi.org/10.1021/bi701278c.
Tong, H., Jiang, Q., Hu, X., Zhong, X., 2020. Occurrence and identification of microplastics in tap water from China. Chemosphere 252, 126493. https://doi.org/10.1016/J.CHEMOSPHERE.2020.126493.
Van der Veken, M., Aertsen, M., Brouwers, J., Stillhart, C., Parrott, N., Augustijns, P., 2022. Gastrointestinal fluid volumes in pediatrics: a retrospective MRI study. Pharmaceutics 14 (9), 1935.
Vivian, J.T., Callis, P.R., 2001. Mechanisms of tryptophan fluorescence shifts in proteins. Biophys. J. 80, 2093–2109.
World Health Organization, 2022. Dietary and Inhalation Exposure to Nano-And Microplastic Particles and Potential Implications for Human Health.
Yu, Y., Luan, Y., Dai, W., 2022. Dynamic process, mechanisms, influencing factors and study methods of protein corona formation. Int. J. Biol. Macromol. 205 731–739.
Zhang, Y., Casabianca, L.B., 2018. Probing amino acid interaction with a polystyrene nanoparticle surface using Saturation-Transfer Difference (STD)-NMR. J. Phys. Chem. Lett. 9, 6921–6925. https://doi.org/10.1021/acs.jpclett.8b02785.
Zhou, X., Wang, J., Li, H., Zhang, H., Hua-Jiang, Zhang, D.L., 2021. Microplastic pollution of bottled water in China. J. Water Process Eng. 40, 101884 https://doi.org/10.1016/J.JWPE.2020.101884.
Zuccarello, P., Ferrante, M., Cristaldi, A., Copat, C., Grasso, A., Sangregorio, D., Fiore, M., Oliveri Conti, G., 2019. Exposure to microplastics (<10 μm) associated to plastic bottles mineral water consumption: the first quantitative study. Water Res. 157, 365–371. https://doi.org/10.1016/J.WATRES.2019.03.091.